A Light Fixture Color Temperature and Color Rendering Index Measuring Device

Gianluca Hiss Garbim, Luis Carlos Mathias, André Massami Assakawa and Taufik Abrão

arXiv:2602.21163v1 [eess.IV] 24 Feb 2026

Abstract—The correlated color temperature (CCT) and color rendering index (CRI) of artificial light sources are important because they have implications for human biology and professional applications. Although CCT information is generally available for commercial lamps, CRI is commonly not reported. In addition, devices measuring these parameters are difficult to access as they require a spectrophotometer, a commonly expensive device. In this context, the present work designs and builds a meter in detail, from the structural part of the equipment, interface with sensors, calculation, to the compensation algorithms implementation, aiming to build dedicated functionalities of a spectrophotometer, which is designed without the use of optical lenses. In addition to simplifying the device, this approach allows measurements free from dispersions caused by chromatic aberrations typical of optical lenses. The prototype obtained proved to be effective, capturing the spectral power distributions of various light sources and calculating their CCT and CRI.

Index Terms—color rendering index, color temperature, meter, spectrophotometer

I. Introduction

IN fact, lighting directly affects biological processes, such as the human circadian rhythm [1]. In this context, artificial lighting can harm the quality of rest, professional work, sales, emotions, even affecting the perception of sweet and bitter flavors [2].

A way to evaluate the quality of a light source is by its color temperature, which defines how much warmer or colder the light source is. However, this parameter alone does not measure the quality of color reproduction in a environment [3]. Objects illuminated by a lamp with high color rendering would imply that most people would describe them as having a natural and pleasant appearance. On the other hand, if illuminated with an inappropriate lamp, objects would take on a less familiar and distorted appearance.

Among the applications in which adequate color reproduction is essential, it is possible to mention any activity that involves the careful choice of colors such as photography, graphic design, lighting, fine arts, as well as those in which the identification of natural processes and organisms, requires attention to color in a controlled environment. One example is the work of [4], which uses neural networks to optimize the light source spectrum for detecting oral lesions in dental applications.

One way to measure this aspect is by the color rendering index (CRI), which is a parameter that consists of comparing the color reproduction of the test light source with a reference source, commonly a model of sunlight. It is based on mathematical comparisons with the expected color curves, in which it is computed in a single numerical value, with the best possible value being 100 % and the worst ones being able to assume negative values [5]. Although it possesses limitations such as the discontinuity in the color temperature of 5000 K and the reduced number of samples [6], it satisfactorily fulfills the role of measuring the naturalness of the color reproduction of an artificial light source [7]. For example, this parameter is even used in the design of visible light communication systems, as in addition to transmitting data, the luminaire must be able to illuminate [8].

However, in many countries, deficiencies (and even the absence) of regulations and legislation related to lighting quality result in great difficulty in predicting the quality of a luminaire. In most cases, this information does not exist for commercial lamps. Added to this fact, CRI measuring instruments are generally not accessible as they require, for their proper functioning, a spectrophotometer [9].

In the literature there are several works that approach the subject of the construction of spectrophotometers [9], [10]. However, most of them are focused on physical/chemical analysis applications and not on determining the quality of artificial lighting. In these approaches, dispersions in the measurements may occur due to the characteristic of chromatic aberration in optical lenses. This occurs due to the typical variation of the refractive index of the lens material as a function of the wavelength [11]. The work in [12] uses artificial neural networks, image cameras and color samples on printed paper. However it only identifies the light source among those tested, not measuring the color temperature or CRI. To date, no work has been found that fully presents the construction of this type of meter.

In the following, we explicitly address the limitations of existing correlated color temperature (CCT) and CRI measurement devices and explain how the proposed solution overcomes such challenges.

Problem Statement: Despite the critical role that CCT and CRI play in assessing the quality of artificial lighting, existing measurement devices face significant limitations.

G. H. Garbim, L. C. Mathias, and A. M. Assakawa are with the Computer Engineering Coordination, Federal University of Technology - Paraná, Toledo, Paraná, 85902-490, Brazil (e-mail: mathias@utfpr.edu.br).

T. Abrão is with Departamento de Engenharia Elétrica, Universidade Estadual de Londrina, Londrina-Paraná, 86057-970, Brazil

Manuscript received April xx, 2024; revised April xx, 2024.

Firstly, while CCT information is often available for commercial lamps, CRI is frequently not reported, leaving a gap in understanding the color rendering capabilities of these light sources. Secondly, the devices currently available for measuring CCT and CRI, typically require a spectrophotometer, which is an expensive and complex piece of equipment. This inaccessibility restricts the ability of professionals and consumers to evaluate lighting quality effectively. Moreover, many existing spectrophotometers rely on optical lenses, which can introduce chromatic aberrations and distortions in measurements due to variations in the refractive index of the lens material across different wavelengths. This can lead to inaccuracies in the reported CCT and CRI values, further complicating the selection of appropriate lighting solutions.

Proposed Solution: To address these challenges, the proposed work presents a novel lighting quality meter designed to measure CCT and CRI without the use of optical lenses. This innovative approach simplifies the construction of the device, making it more cost-effective and accessible for users. By employing a dedicated spectrophotometer that utilizes alternative optical arrangements, the device minimizes the risk of chromatic aberrations, thereby enhancing measurement accuracy. This cost-effective solution ensures that professionals and consumers can evaluate lighting quality without the financial burden of expensive equipment. The comprehensive design integrates both hardware and software components, allowing the effective capture of spectral power distributions (SPDs) from various luminaires. The meter's calibration process, validated against a commercial spectrophotometer, ensures reliable calculations of CCT and CRI. Ultimately, this solution not only provides a practical tool for measuring lighting quality but also empowers users to make informed decisions regarding artificial light sources, thereby improving their applications in fields such as photography, design, and healthcare.

Thus, this work proposes to comprehensively integrate a software solution and a hardware device composed of a dedicated spectrophotometer for analyzing the light spectrum of luminaires, allowing the determination of the CCT and CRI using accessible materials and equipment. In this sense, this research work has the following goals:

1) prepare a comprehensive review of the quality of artificial lighting, specifically concerning color reproduction;
2) establish two optical geometric arrangements for the construction of the meter, without the use of optical lenses; therefore, of low-cost, simplified construction and without chromatic aberration;
3) determination of construction parameters, analysis of expected accuracy and linearity of measurements;
4) build the meter, from the structural mechanical part, electronic interfaces, calibration and compensation, operating algorithms and calculations of color reproduction quality parameters;
5) carry out measurements of different luminaires to validate the proposed meter.

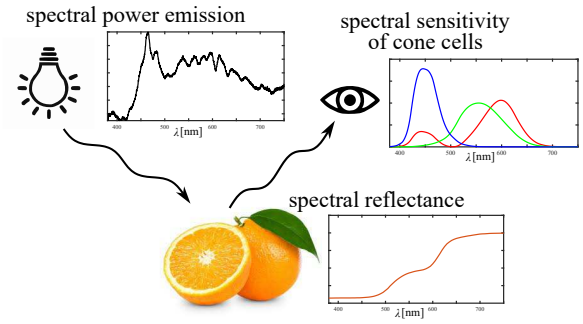


Fig. 1. Color perception process [14], [15].

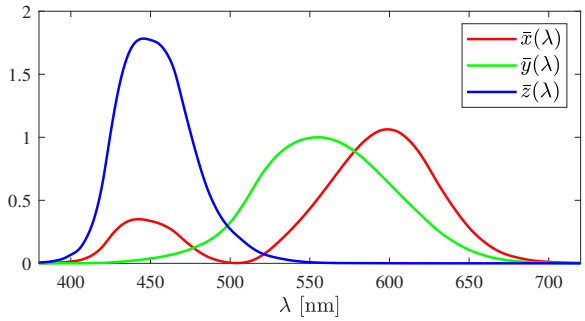


Fig. 2. Color matching functions.

The remainder of this document is organized into five sections. Section II presents the theory of perception and measurement of color reproduction, while Section III analyzes the optical geometry of the meter. Section IV presents details of the building and calibration of the meter prototype, while its results from measuring the lighting quality of different luminaires are presented in Section V. Finally, the Section VI presents the main conclusions of the work.

II. Color reproduction

The human eye has the ability to perceive colors by capturing light, which is commonly composed of different intensities at different wavelengths. In this sense, the spectral power distribution (SPD) is the curve that describes the amount of energy that a light source emits as a function of wavelength. According to Fig. 1, the light perception process can be divided into three stages. Initially, the illuminant with a specific SPD illuminates an object, that has a specific reflectance spectrum. Under suitable lighting, the light reflected by the object is captured by the three types of vision cone cells, each of which has sensitivity in different wavelength ranges [13], [14].

A. Color spaces

Three values, called tristimulus, were developed to represent the stimulus level of each type of cone receptor. In the 1931 International Commission on Illumination (CIE) color model, the tristimulus X, Y, and Z are used

[16]. Y represents luminance, while X and Z represent chromaticity coordinates. The great advantage of this scheme is that, for any luminance value, a plane can represent all possible chromaticities.

Due to the physical distribution of cones in the eye, tristimulus values are affected by the observer's field of vision [17]. To mitigate the influence of this variable, the CIE 1931 establishes a colorimetric standard observer, with the purpose of standardizing an observer's chromatic response to an arc of 2° from the fovea (ocular region where most are concentrated cone cells). To numerically describe this chromatic response, color matching functions $\bar{x}$, $\bar{y}$ and $\bar{z}$ were developed, which are available in the table 2DegStdColObs (2 degree standard color observer) in [16]. These are demonstrated in Fig. 2.

In this way, the tristimulus values X, Y and Z can be defined by product integration between the SPD $S(\lambda)$ of the captured light and the color matching functions:

$$X = \int_{\lambda_\mathrm{l}}^{\lambda_\mathrm{h}} S(\lambda)\,\bar{x}(\lambda)\,d\lambda; \tag{1}$$

$$Y = \int_{\lambda_\mathrm{l}}^{\lambda_\mathrm{h}} S(\lambda)\,\bar{y}(\lambda)\,d\lambda; \tag{2}$$

$$Z = \int_{\lambda_\mathrm{l}}^{\lambda_\mathrm{h}} S(\lambda)\,\bar{z}(\lambda)\,d\lambda; \tag{3}$$

where λ_l represents the shortest wavelength for which the SPD presents information, and λ_h the longest [16]. In this work, the variables that have the subscript $_\mathrm{l}$ and $_\mathrm{h}$ are relative to the lower and upper wavelength limits, respectively.

From X, Y and Z, it is possible to determine the parameters x, y and z that define the chromaticity in the color space:

$$x = \frac{X}{X+Y+Z}; \tag{4}$$

$$y = \frac{Y}{X+Y+Z}; \tag{5}$$

$$z = \frac{Z}{X+Y+Z} = 1 - x - y. \tag{6}$$

where the value of z can be deduced from x and y, it is generally discarded in the representations, giving rise to the CIE 1931 color space.

A notable difficulty of the CIE 1931 color space is that it is not uniform, that is, the Euclidean distances between points on the graph are not proportional to differences in the observer's visual perception. As a solution, the uniform color space (UCS) was developed, which presents chromatic distances proportional to those perceived by the human eye in coordinates u and v [18]. This was simplified in 1937 and became the standard recommended by the CIE in 1960 [19]. This can be obtained by transforming chromaticities:

$$u = \frac{4x}{12y - 2x + 3}; \tag{7}$$

$$v = \frac{6y}{12y - 2x + 3}. \tag{8}$$

Later, the CIE 1964 color space was developed to enable the calculation of color differences without the need to maintain constant luminance Y. This uses a luminosity index $W^\star$ together with the chromaticity coordinates $U^\star$ and $V^\star$ [19]. For the purpose of lighting quality analysis, it is possible to transform colorimetric data to the CIE 1964 color space through the following relationships:

$$W^\star = 25Y^{\frac{1}{3}} - 17; \tag{9}$$

$$U^\star = 13W^\star\,(u_k - u_r)\,; \tag{10}$$

$$V^\star = 13W^\star\,(v_k - v_r)\,; \tag{11}$$

in which u_r and v_r represent the chromaticity of the reference, u_k and v_k represent the chromaticity of the light source being analyzed, all from the CIE 1960 color space. With the reference and illuminant data transformed into this color space, color differences can be calculated.

B. Correlated color temperature

A blackbody is a theoretical object that absorbs all incident electromagnetic radiation, emitting radiation [20]. Taking into account that LED and fluorescent lamps do not have the same SPD as black bodies, the correlated color temperature (CCT) was developed to relate the light source to the nearest black body. However, contrary to the conventional temperature scale, the color temperature scale goes from warm (lower temperatures) to cool (higher temperatures) [21]. For example, the color temperature of sunlight varies from warmer values at sunrise and sunset (about 3000 K) to cooler values near midday (in the range of 5000 and 6000 K).

Two methods to approximate the CCT are described in [22]. The first uses a polynomial equation:

$$T_\mathrm{cct}(x,y) = -449n^3 + 3525n^2 - 6823.3n + 5520.33; \tag{12}$$

in which $n = \frac{x-x_e}{y-y_e}$ with epicenter at $x_e = 0.3320$ and $y_e = 0.1858$ [23]. However, this presents a large error for very high CCTs [22]. The second uses the following sum of exponentials equation:

$$T_\mathrm{cct}\,(x,y) = A_0 + A_1 \exp\left(-\tfrac{n}{t_1}\right) + A_2 \exp\left(-\tfrac{n}{t_2}\right) + A_3 \exp\left(-\tfrac{n}{t_3}\right); \tag{13}$$

considering the epicenter at $x_e = 0.3366$ and $y_e = 0.1735$; and the coefficients, for lighting purposes, between 3000 and 50000 K, are $A_0 = -949.8631$, $A_1 = 6253.80338$, $A_2 = 28.70599$, $t_1 = 0.92159$, $t_2 = 0.20039$ and $t_3 = 0.00004$.

C. Standard illuminant

The daylight is chosen as the reference because it is a lighting condition commonly perceived as natural and pleasant, while blackbody radiators are chosen for lower temperatures because they present similar behavior to incandescent and halogen lamps. The spectral energy distribution of a blackbody can be approximated as a function of its CCT. Therefore, Planck's radiation law is a suitable approximation for the SPD of a lamp with a

color temperature below 5000 K (standard A illuminant) [20], [24]:

$$S_{\mathrm{a}}(\lambda) = \frac{c_1}{\lambda^5} \cdot \left[\exp\left(\frac{c_2}{\lambda} \cdot T_{\mathrm{cct}}\right) - 1\right]^{-1} \qquad \left[\frac{W}{m^3}\right]; \quad (14)$$

where $c_1 = 3.7418 \times 10^{-16}$ and $c_2 = 1.4388 \times 10^{-2}$ are the Planck radiation constants.

For CCTs above 5000 K, it is possible to approximate the SPD of the reference source using the D series illuminant through the composition of three SPDs, S_0, S_1 and S_2, available in the CIEDaySN table in [16], which were obtained from empirical measurements. S_0 corresponds to the average of all SPD sunlight samples; S_1 to yellow-blue variations due to the presence of clouds; and S_2 to pink-green variations due to the presence of water vapor. In this approach, the SPD is:

$$S_{\mathrm{d}}(\lambda) = S_0(\lambda) + M_1 S_1(\lambda) + M_2 S_2(\lambda); \quad (15)$$

in which the coefficients M_1 and M_2 are determined by:

$$M_1 = \frac{-1.3515 - 1,7703 x_{\mathrm{d}} + 5.9114 y_{\mathrm{d}}}{0.0241 + 0.2562 x_{\mathrm{d}} - 0.7341 y_{\mathrm{d}}}; \quad (16)$$

$$M_2 = \frac{0.030 - 31,4424 x_{\mathrm{d}} + 30.0717 y_{\mathrm{d}}}{0.0241 + 0.2562 x_{\mathrm{d}} - 0.7341 y_{\mathrm{d}}}; \quad (17)$$

where the values of x_{d} and y_{d} originate from the chromaticities defined by the CIE 1931 color space, which are determined by their correlated color temperature T_{cct}:

$$y_{\mathrm{d}} = -3x_{\mathrm{d}}^2 + 2.87 x_{\mathrm{d}} - 0.275. \quad (18)$$

For 4000 K $\leq T_{\mathrm{cct}} \leq$ 7000 K we have:

$$x_{\mathrm{d}} = 0.244063 + 0.09911\frac{10^3}{T_{\mathrm{cct}}} + 2.9678\frac{10^6}{T_{\mathrm{cct}}^2} - 4.6070\frac{10^9}{T_{\mathrm{cct}}^3}; \quad (19)$$

already for 7000 K $\leq T_{\mathrm{cct}} \leq$ 25000 K:

$$x_{\mathrm{d}} = 0.237040 + 0.24748\frac{10^3}{T_{\mathrm{cct}}} + 1.9018\frac{10^6}{T_{\mathrm{cct}}^2} - 2.0064\frac{10^9}{T_{\mathrm{cct}}^3}. \quad (20)$$

Fig. 3 depicts the SPDs, normalized by the peak, for standard illuminants A for CCTs of 3000, 4000 and 5000 K (A30, A40 and A50) and also for standard illuminants D for CCTs of 5000 and 6504 K (D50 and D65). As expected, and in general, the increase in CCT implies an increase in intensity at shorter wavelengths compared to longer wavelengths. Another detail is that for the same CCT of 5000 K, the D50 illuminant appears to follow the behavior of the A50 illuminant curve from approximately 450 nm onwards.

D. Metamerism and chromatic adaptation

It is possible for light sources with different SPDs to present equal chromaticities. This behavior is called metamerism. For example, a blackbody whose SPD is represented by a curve can generate the same chromaticity as an LED light source with several peaks spread across the spectrum. However, the perceived color reproduction will still be different [25].

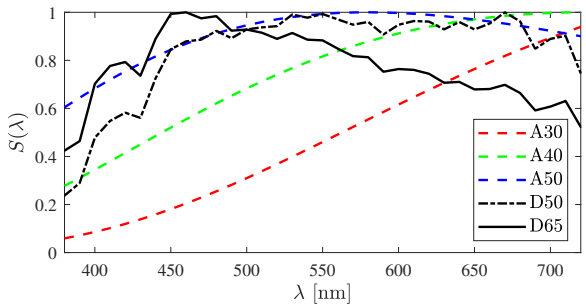


Fig. 3. Normalized SPD of standard type A and D illuminants.

Another phenomenon that affects color perception is chromatic adaptation. Process carried out by the human visual system that adapts the perception of a color to match what is expected. For example, a painting observed under midday sunlight has very different colors than the same one observed under sunset lighting. Our visual system, however, adapts these colors so that they maintain their relative differences regardless of these variations [26].

Numerically, chromatic adaptation can be carried out using the u and v parameters of the CIE 1960 color space [27]:

$$c = \frac{4 - u - 10v}{v}; \quad (21)$$

$$d = \frac{1.708v + 0.404 - 1.481u}{v}. \quad (22)$$

These are calculated both for the light source under evaluation, c_k and d_k, and for the reference samples, c_r and d_r. Thus, the new chromaticity coordinates for a given sample i can be defined by:

$$u'_{k,i} = \frac{10.872 + 0.404\frac{c_r}{c_k}c_{k,i} - 4\frac{d_r}{d_k}d_{k,i}}{16.518 + 1.481\frac{c_r}{c_k}c_{k,i} - \frac{d_r}{d_k}d_{k,i}}; \quad (23)$$

$$v'_{k,i} = \frac{5.520}{16.518 + 1.481\frac{c_r}{c_k}c_{k,i} - \frac{d_r}{d_k}d_{k,i}}; \quad (24)$$

in which $u'_{k,i}$ and $v'_{k,i}$ represent the adapted colors and $d_{k,i}$ refers to the product of the SPD of the light evaluated light source and the reflectance of sample i.

E. Color rendering index

The color rendering index (CRI) evaluates, through comparison with a reference, the quality of color reproduction of artificial light sources. Conventionally, the appearance of predefined color samples under the effect of a standard illuminant is compared with the reproduction of the illuminant being tested. The differences are described by the distance between the sample illuminated by the reference lamp and the lamp under evaluation in terms of chromaticity and luminance [27].

This way, it is possible to calculate the CRI for specific samples, which are described by a specific reflectance function. For each sample, the distance between the color generated by the test source and the color generated by the

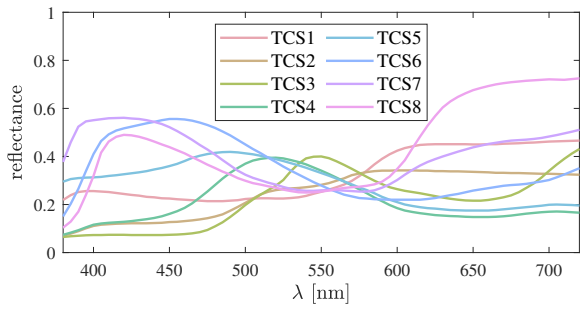


Fig. 4. Reflectances of test color samples [16].

reference (both in the CIE 1964 color space) is calculated [27]:

$$\Delta E_i = \sqrt{\left(\Delta U^*_{r,i} - \Delta\, U^*_{k,i}\right)^2 + \left(\Delta V^*_{r,i} - \Delta V^*_{k,i}\right)^2 + \left(\Delta W^*_{r,i} - \Delta W^*_{k,i}\right)^2}; \tag{25}$$

then generating the CRI value for this sample:

$$R_i = 100 - 4.6\Delta E_i. \tag{26}$$

To calculate the average CRI R_a of a light source, eight test samples (TCS) must be illuminated by the source under evaluation and, subsequently, by the reference source [27]. This process can occur in a simulated way, applying the SPD measured directly from the light source to be tested and the SPD from the reference source, both on the reflectance functions of each sample (see Fig. 4). Thus, the general value of the CRI can be obtained from the arithmetic mean:

$$\mathrm{R}_a = \frac{1}{8}\sum_{i=1}^{8} R_i. \tag{27}$$

It should be noted that the CRI R_a has a maximum value of 100 %, in which the lamp reproduction is virtually identical to that of the chosen reference. At CRIs below this value, the difference to 100 is proportional to the average magnitude of the color differences. In practice, differences of the order of 5 are not noticeable to an observer [27].

III. Meter Optical geometry

SPD can be measured using a device called a spectrophotometer. In general, this can be built using a light scatterer, lenses, and photosensors [9], [10]. As a disperser, diffraction gratings are commonly used, which are devices that have hundreds to thousands of slits per millimeter. As photosensors, a linear CCD (charge-coupled device) sensor can be used, a device that has thousands of photosensors arranged in a line, which are generally used in barcode reader devices [28].

As in this work, the light intensities generated by the luminaires are much greater than those commonly used in chemical analysis spectrophotometers, the project can become simplified and more compact without the necessity of optical lenses. This approach has the advantage that measurements do not suffer from chromatic aberrations, which are common when optical lenses are used.

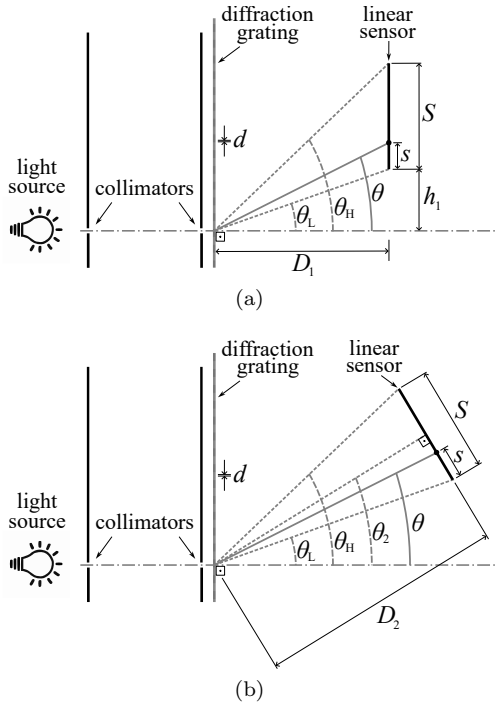


Fig. 5. Geometry of the first arrangement in (a) and the second arrangement in (b).

As shown in Fig. 5(a), after the collimating bulkheads, the light passes through the diffraction grating in several slits, and in each slit it is diffracted at different angles. This causes the light rays of the same wavelength, which reach a point on the sensor s, to travel different distances and thus reach a point s with different time delays. Considering the wave characteristic of light, destructive or constructive interference may occur if the delays are close to odd multiples or even multiples of half a wavelength, respectively [29]. Thus, an interference figure is created along the linear CCD sensor, where the position of the maximum point s, where constructive interference occurs, depends on the wavelength of the light that falls on the diffraction grating [29]:

$$d\sin\theta = m\lambda; \tag{28}$$

in which d is the spacing between the slits, θ the angle between the central axis and the diffracted rays, m the order of the position being measured, and λ the wavelength being evaluated.

In this way, each wavelength will have a different maximum point on the sensor, allowing the intensities to be discriminated depending on the wavelength, i.e., the SPD. In this sense, this section models and adequately designs the arrangement of the components of a spectrophotometer, considering two distinct geometric arrangements. In both analyses, the objective is to use the entire detector length of the linear CCD sensor in order to obtain a greater number of detectors per wavelength range analyzed. This directly implies a greater resolution of the meter, increasing the number of points of the SPD curve captured.

A. CCD sensor parallel to the diffraction grating

This first approach considers a classic arrangement that is very common in the literature [29]. The angles θ_l and θ_h can be determined by (28) for λ_l and λ_h. The first order ($m = 1$) will be considered, as it has the advantage of presenting greater angular dispersion and, consequently, enabling a smaller distance between the diffraction grating and the linear CCD sensor given the total range of λ to be captured.

From the smaller right triangle in Fig. 5(a), it is possible to determine the height h_1:

$$h_1 = D_1 \tan\theta_\mathrm{l} \tag{29}$$

and from the larger right triangle we have:

$$S + h_1 = D_1 \tan\theta_\mathrm{h}; \tag{30}$$

where S is the useful length of the linear CCD sensor.

By applying (29) to (30), it is possible to determine the distance:

$$D_1 = \frac{S}{\tan\theta_\mathrm{h} - \tan\theta_\mathrm{l}}; \tag{31}$$

finally allowing us to determine the height h_1 from (29).

B. Linear CCD sensor inclined to the diffraction grating

In this second arrangement, the linear CCD sensor is positioned perpendicular to a medium angle:

$$\theta_2 = \frac{\theta_\mathrm{h} + \theta_\mathrm{l}}{2}. \tag{32}$$

According to Fig. 5(b), the sensor forms the base of an isosceles triangle. Through the upper right triangle, it is possible to obtain the last parameter of the project:

$$D_2 = \frac{S}{2\tan(\theta_\mathrm{h} - \theta_2)}. \tag{33}$$

Thus, it appears that the calculations for the design of this second arrangement are more expeditious, compared to the previous one.

C. Linearity analysis

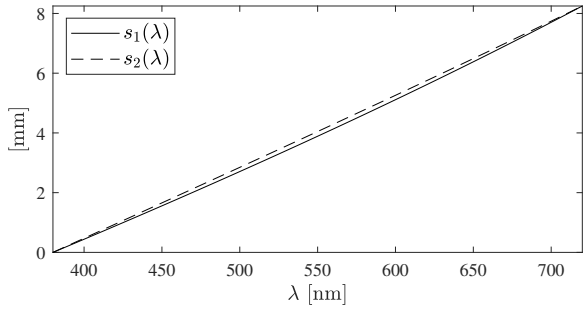
Nonlinearities directly imply distortion of the captured SPD, propagating an error in the calculation of the CCT and CRI. In this sense, it is possible to evaluate the linearity between the position s of the photosensors of the linear CCD sensor and the wavelength λ to be detected. Thus, from the analysis of Fig. 5(a), (30) and (28), it is possible to obtain for the first arrangement:

$$s_1(\lambda) = D_1 \tan\left(\sin^{-1}\frac{\lambda}{d}\right) - h_1; \tag{34}$$

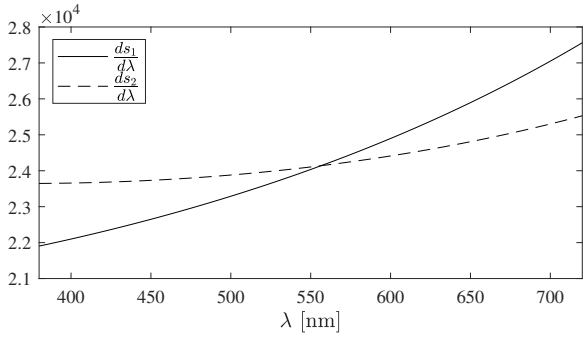
where λ is the analyzed wavelength.

Using Fig. 5(b) and (33), a similar analysis can be done for the second arrangement:

$$s_2(\lambda) = \frac{S}{2} - D_2 \tan\left(\theta_2 - \sin^{-1}\frac{\lambda}{d}\right). \tag{35}$$



(a)



(b)

Fig. 6. Position of the maximum point in (a) and its derivative in (b), both as a function of lambda.

If it is exactly linear, the slope must be constant throughout λ. Therefore, the derivative as a function of wavelength can be applied to (34) and (35):

$$\frac{ds_1}{d\lambda} = \frac{dD_1}{(d^2 - \lambda^2)\sqrt{1 - \frac{\lambda^2}{d^2}}} \tag{36}$$

and

$$\frac{ds_2}{d\lambda} = \frac{D_2 \sec^2(\theta_2 - \sin^{-1}\frac{\lambda}{d})}{d\sqrt{1 - \frac{\lambda^2}{d^2}}}. \tag{37}$$

Therefore, neither arrangement is exactly linear. However, as the values of λ are much smaller compared to the values of d, it is possible to verify that the variation of (36) and (37) as a function of λ are small. Thus, considering the project of this work, for a wavelength range between 380 and 720 nm, a diffraction grating with 600 slits per mm, i.e., $d = 1.666$ µm, and a CCD sensor length of $S = 8.25$ mm [28], Fig. 6(a) was generated, of the maximum position s as a function of λ. It shows that the second arrangement has better linearity compared to the first arrangement. This is corroborated by Fig. 6(b), of its derivatives, which confirms a smaller variation in the slope rate for the second arrangement. Therefore, as it presents better linearity characteristics, this arrangement was chosen for the development of this work.

D. Resolution as a function of collimator aperture

The resolution of the interference figure projected on the linear sensor is dependent on the aperture a of the collimator that allows light to enter the diffraction grating

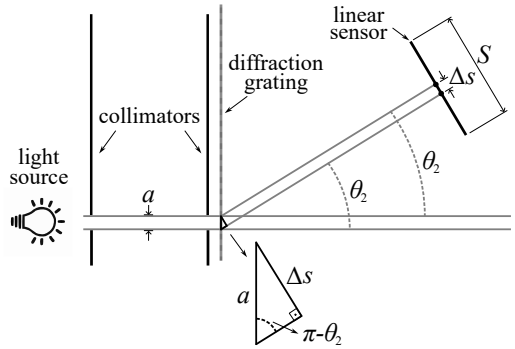


Fig. 7. Resolution as a function of collimator aperture.

[29]. This analysis can be best exemplified in Fig. 7. The useful length S of the linear sensor must capture the entire range from λ_l to λ_h. Considering δ as the required wavelength resolution of the spectrophotometer and that the variation of the position on the sensor Δs is approximately linear in relation to the variation of the light wavelength, we have:

$$\Delta s \simeq \frac{\delta S}{\lambda_h - \lambda_l}. \tag{38}$$

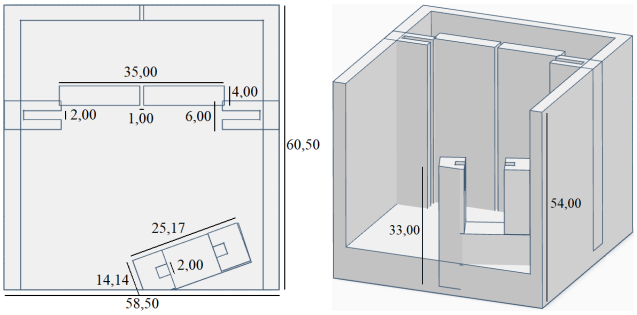
Thus, based on the right-angled triangle in Fig. 7, it is possible to establish the following relationship for determining the aperture:

$$a \simeq \frac{\delta S}{(\lambda_h - \lambda_l)\sin(\pi - \theta_2)}. \tag{39}$$

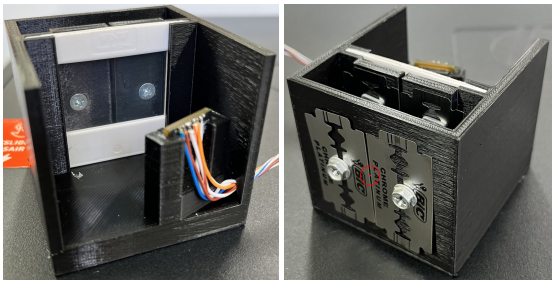
Thus, a smaller aperture implies a higher resolution in the measurement; however, it also reduces the amount of captured light. This last consequence is not a problem for the application of this work since in tests carried out, the light sources presented sufficient luminous power to excite the linear CCD sensor, even with apertures of a few tenths of a millimeter.

IV. Construction and implementation

Part of the spectrophotometer design parameters were presented in subsection III-C, which allows, through (32) and (33), to determine the average angle $\theta_2 = 33.8°$ and the distance $D_2 = 3.79$ cm, respectively. Therefore, according to Fig. 8(a), the design of the structural part of the prototype was carried out using 3-D printing. Fig. 8(b) shows the structure printed with Polylactic Acid (PLA) material, highlighting the fitting positions for the diffraction grating, the linear CCD sensor and the two pairs of blades that function as collimators. The 3-D printer used was the Creality® Ender-3, which the manufacturer guarantees accuracy of ±0.1 mm. The glass protection of the linear CCD sensor was removed to avoid possible reflections, which could distort the measurements. Considering an expected resolution of $\delta = 2.5$ nm, the slot width of the screens was adjusted to $a \simeq 0.18$ mm, taking into account (39). Also, an "L"-shaped cover was developed, which can be removable, protecting the device from ambient light in order to only allow, through the collimators, the entry of the light that must be analyzed.



(a)



(b)

Fig. 8. Geometry and dimensions in mm of the constructed prototype in (a), and internal photos in (b). It is possible to see the installation of the stainless steel blades as collimators, the housings of the diffraction grating, and the CCD linear sensor. The red circle in the photo highlights the opening for light entry.

A. Sensor and microcontroller interface

According to Fig. 9(a), a microcontroller (µC) was used as an interface between the TCD1103 sensor and a personal computer (PC). The OS pin (output signal) is an analog output with a voltage proportional to the inverse of the light intensity captured by each sensor. This signal is updated depending on the digital signals ICG (integration clear gate), SH (shift gate), and ϕM (master clock) that must be generated by µC. Three pins are used to power the sensor (SS, V_{DD} and V_{AD}). The remaining pins are unconnected (NC). After the ICG signal rise sequence (see Fig. 9(b)), OS presents the reading from the first photosensor. Every two ϕM cycles, the TCD1103 switches the reading to the next photosensor. According to [28], the set of photosensors protected from light, signals ranging from D16 to D28, allows the calibration of the dark level, while the effective outputs of the photosensors represent the signals between S1 and S1500.

According to Fig. 9(b), the timing requirements required by the TCD1103 are very restricted. Therefore, the µC model STM32F103C8T6 from the manufacturer STMicroelectronics was used at the maximum clock frequency of 72 MHz of its ARM Cortex M3 core. A channel of a timer peripheral was configured to generate a pulse width modulated (PWM) signal with a cyclic ratio of 50%, which corresponds to the rectangular wave of the ϕM signal. The interrupt handling function of this timer, associated with an algorithm, allowed the generation of SH and ICG signals. The implemented times are t1 = 124 t2 = 2500, t3 = 10200, t4 = 7900 and t5 = 2500, all in nanoseconds

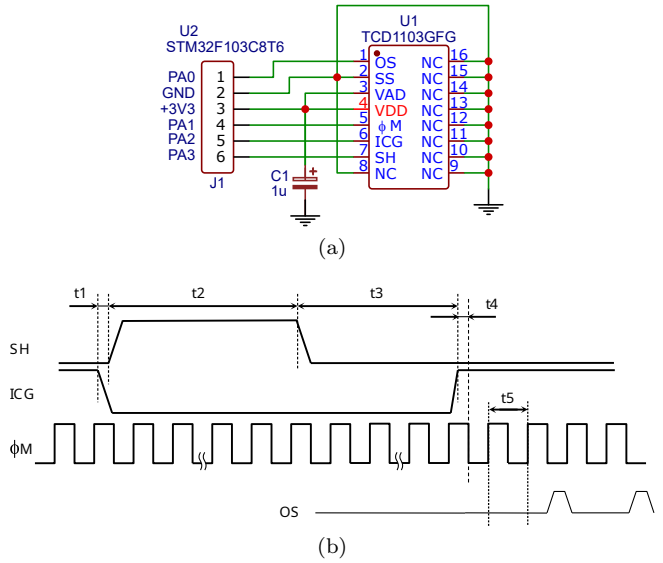


Fig. 9. Electrical diagram in (a) and timing diagram in (b), both of the TCD1103 and µC sensor interface.

and within the limits specified in [28]. The analog OS signals were captured using an internal analog-to-digital converter (ADC) channel of µC with 12 bit resolution, which is stored in a vector to later be transmitted to the PC through a serial communication interface.

A longer interval between positive SH pulses t_{int} defines a longer capture time in the CCD sensors [28]. Through tests, a $t_{int} \approx 250$ ms allowed adequate capture of the SPD at light intensities starting from 200 lux. For the lowest power lamp analyzed, the 15 W incandescent, this was equivalent to a distance of approximately 30 cm from the prototype apperture.

B. Responsivity compensation of linear CCD sensors

The linear CCD sensor used in this work is model TCD1103 from the manufacturer TOSHIBA, which has 1500 sensor elements composed of high sensitivity PN photodiodes. Its responsiveness curve is shown in [28], as well as its adjustment by a 5th order polynomial function by:

$$R_{\text{ccd}}(\lambda) = -1.783\times10^{32}\lambda^5 + 4.289\times10^{26}\lambda^4 - 3,919\times10^{20}\lambda^3 + 1.575\times10^{14}\lambda^2 - 2.170\times10^{7}\lambda + 0.2012. \quad (40)$$

C. Calibration

The calibration of the position s of the photosensors as a function of the wavelengths (x scale of the SPDs) took place based on measurements from a commercial spectrophotometer model FLAME-T-XR1-ES from the manufacturer Ocean Optics, considering the peaks of the SPDs of two high-brigness LEDs with colors blue and red. In this way, and according the Fig. 10, the wavelength of the first CCD sensor was adjusted to 391 nm and the last one to 723 nm. Both calibration and measurements were performed in a temperature-controlled laboratory at 20°C. It is important to maintain this control, otherwise

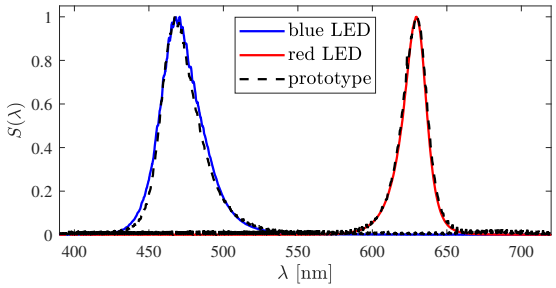


Fig. 10. Calibration of the x-axis of the prototype by comparing the measurements of two colored LEDs made by a commercial spectrophotometer..

the PLA material may expand or contract, modifying the geometry of the structure at different temperatures.

D. General description of operation

Given what has been presented, the functioning of the meter can be summarized as follows:

1) The light emitted by the luminaire to be analyzed is collimated by two pairs of parallel screens before reaching the diffraction grating;
2) The diffraction grating decomposes the captured light, separating the wavelength bands in an angular way, generating a colored beam of light;
3) The colored light beam reaches the photosensors of the CCD sensor which, in a scanning scheme, converts the intensities into analog voltage levels;
4) The combination of digital synchronization and clock signals generated by µC, switches the analog intensity signals of each sensor;
5) µC captures these signals using an ADC;
6) These sampled signals are then sent to the PC, on which the CCT and CRI estimation algorithms are executed.

E. Lighting quality analysis

On the PC, the CCT and CRI are calculated according to the following steps:

1) In the intensity vector captured from the linear CCD sensor, dark calibration is performed, which consists of subtracting the average levels of the dark photosensors from the signals from the effective photosensors;
2) To minimize distortions in the captured intensities as a function of λ, the inverse of (40) is applied, defining the SPD of the light source to be evaluated;
3) The CCT is determined with (12) or (13);
4) According to the CCT, a reference SPD is generated using blackbody radiation for values less than 5000 K (with (14)) or the standard illuminant D for values equal to or greater than 5000 K (with (15), (16) and (17), (19) or (20), and (18));
5) The tristimulus values are calculated, and normalized to $Y = 100$, for the evaluated illuminant, for the reference illuminant, and for the eight TCSs with (1), (2) and (3);

6) Tristimulus values are transformed to the CIE 1931 color space (with (4) and (5)) and then to the CIE 1960 UCS uniform color space (with (7) and (8));
7) Chromatic adaptation is applied to each sample with (21), (22), (23) and (24);
8) The colorimetric information of the samples is transformed to the CIE 1964 color space with (9), (10) and (11);
9) The value R_i is calculated for each sample with (26), through the colorimetric distances ΔE_i with (25);
10) The mean of the R_i values with (27) is the CRI R_a.

V. Results

Table I presents information and results for the CCT and CRI of fourteen light sources analyzed by the developed meter. For comparison purposes, the nominal CCTs (defined by the manufacturer) of the lamps were identified. In some cases, the manufacturer does not present this information on the product. For all light sources analyzed, nominal CRI information was also not found. The fact that these important parameters are often neglected corroborates the need of the meter developed in this work.

The biggest discrepancies were presented for the CCT, with a minimum, average, and maximum difference of 10.8%, 24.6% and 37.0%. This can be attributed to considering the nominal value as a comparison, which may not be the most accurate, due to several factors, such as inconsistencies in the information provided by the manufacturer to the aging of the lamp.

For comparison purposes, the average values of twenty-nine fluorescent lamps, four incandescent lamps, two halogen lamps, and four LED lamps were considered in [3], [6] and [30]. Regarding the CRI, the measured values were more coherent compared to the theoretical values, presenting a minimum, average, and maximum difference of 0.06%, 3.2% and 8.0%, validating the developed meter. As theoretically expected, halogen lamps, followed by incandescent lamps, have the highest CRIs. LED-based lamps had slightly lower CRIs compared to the fluorescent lamps analyzed [31]. It is also found that the LED flashlights of smartphones evaluated have a cold color temperature and lower color rendering indices when compared to the other LED lamps analyzed.

Fig. 11 shows the measured SPDs, normalized by the peak. In order to not make visualization difficult, the results are presented for the first five light sources in Table I. A similar shape to the blackbody spectrum is observed for the halogen lamp and the incandescent lamp. It is also possible to notice the difference in format between the two LED lamps, with the warmer one (T8 LED) having relatively greater magnitudes in the red region compared to the E27 LED Ourolux 6 W. In Figs. 12(a) and 12(b), the chromaticity coordinates of these lamps are printed to visually demonstrate the performance of each lamp. The coordinates of the points in these two graphs confirm that the halogen and incandescent lamps have warmer colors (showing smaller CCTs), the T8 and fluorescent

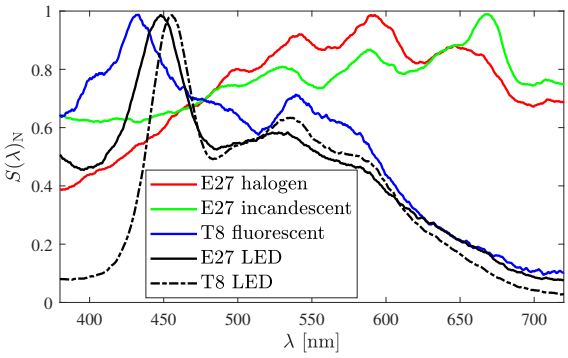


Fig. 11. SPDs measured by the prototype of the first five lamps in Table I.

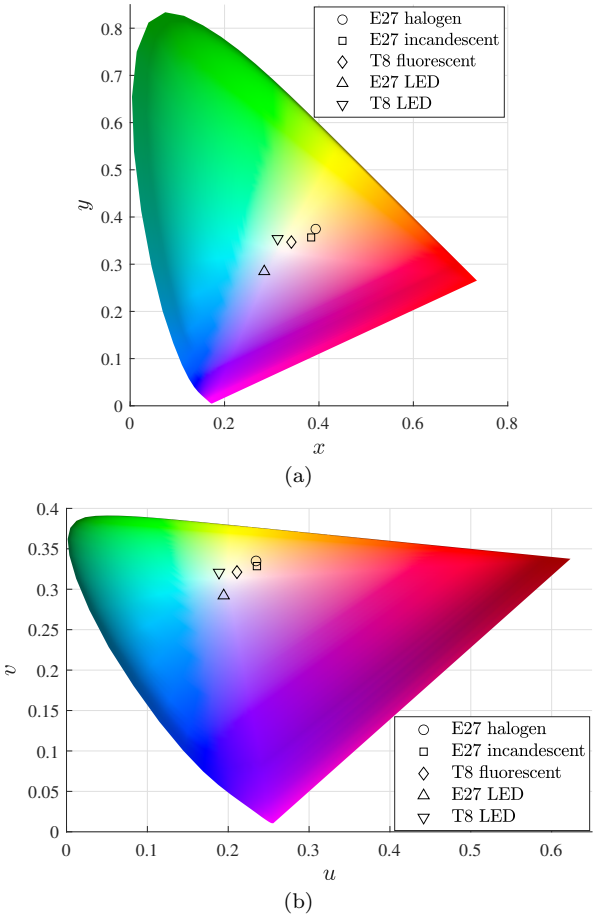


Fig. 12. Results for CIE 1931 color space in (a) and for CIE 1960 UCS color space in (b), for the first five lamps in Table I.

LEDs are more neutral, and the E27 LED Ourolux 6 W has the coldest color (higher CCT) among the luminaires considered.

VI. Conclusion and Future Directions

This research successfully designed, constructed, and validated a low-cost, high-accuracy light fixture color temperature (CCT) and color rendering index (CRI) measuring device. The device utilizes a novel optical geometry, eliminating the need for expensive optical lenses and mitigating chromatic aberration, issues that are common in

TABLE I
Prototype measurement results

Lamp type	Brand	Power [W]	CIE 1931	CIE 1960	R_a [%]		CCT [K]	
			(x, y)	(u, v)	measure	[3], [6], [30]	measure	nominal
E27 halogen	Ourolux	70	(0.393, 0.375)	(0.234, 0.335)	97.76	97,0	3703	2700
E27 incandescent	Empalux	15	(0.384, 0.357)	(0.236, 0.329)	92.41	93.8	3775	-
T8 fluorescent	G-light	36	(0.342, 0.347)	(0.211, 0.321)	90.67	82.7	4815	6400
E27 LED	Ourolux	6	(0.284, 0.285)	(0.194, 0.292)	89.90		7286	6500
T8 LED	Osram	18	(0.312, 0.354)	(0.189, 0.321)	88.98		5108	6500
SPOT LED	Hoya	5	(0.342, 0.368)	(0.203, 0.328)	82,84		5173	4000
LED strip white	-	-	(0.358, 0.319)	(0.203, 0.328)	79.32		4326	-
LED strip white warm	-	-	(0.351, 0.347)	(0.217,0.322)	88,78	85.5	4762	3000
E27 LED	Onlux	4.9	(0.294, 0.316)	(0.189, 0.306)	83.55		7836	6500
E27 LED	Taschibra	9	(0.359, 0.356)	(0.219, 0.326)	89.74		4527	3000
E27 LED	Taschibra	4.9	(0.297, 0.335)	(0.185, 0.313)	83.00		7319	6500
E27 LED	Ourolux	9	(0.287, 0.301)	(0.190, 0.299)	86.23		8790	6500
smartphone LED flashlight	Xiami Redmi 12C	-	(0.307, 0.347)	(0.187, 0.318)	69.80	-	6673	-
smartphone LED flashlight	Motorola E7 plus	-	(0.304, 0.348)	(0.185, 0.318)	72.20	-	6816	-

traditional spectrophotometers. This design significantly reduces cost and complexity while maintaining accuracy comparable to established commercial devices.

The prototype effectively captures spectral power distributions (SPDs) across a broad wavelength range. Linearity analysis demonstrated that the chosen optical arrangement provides suitable accuracy. The device underwent rigorous calibration using known SPDs from commercial LEDs verified by a commercial spectrophotometer. Subsequent measurements from various light sources, including halogen, incandescent, fluorescent, and LED, were used to evaluate the performance of the developed meter.

The results obtained for CRI values showed excellent agreement (within a maximum difference of 8.0%) with established theoretical values and values reported in relevant literature. CCT measurements, while exhibiting higher deviations (reaching an average value of 24.6%), are likely influenced by the use of nominal manufacturer values for comparison; more precise measurements could be made using calibrated standard lamps. Small discrepancies in the CCT may be attributed to the inaccuracy of the nominal values and variations between manufactured batches, among others. However, the consistency of the CRI values strongly validates the accuracy of the proposed spectrophotometric design and its implementation.

Looking ahead, there is a promising path for enhancing the system's calibration techniques to further boost CCT accuracy. Moreover, the software and display screen for displaying the results could be integrated with the developed spectrophotometer into a single stand-alone device, allowing greater versatility without needing an attached personal computer. Additional testing and analysis of a wider range of applications, such as artificial lighting for agriculture, for example, could also strengthen the conclusions presented, instilling a sense of optimism about the future potential of the device.

This cost-effective and accurate device is not just a research tool, but a practical asset for the field of lighting quality assessment. It offers a reliable tool for researchers, manufacturers, and lighting designers, reassuring them of its usability. The methodology and results presented here lay a solid foundation for further advancements in low-cost, high-accuracy lighting metrology.

Acknowledgment

This work was supported in part by the National Council for Scientific and Technological Development (CNPq) of Brazil under Grant 314618/2023-6 and 405301/2021-9, and by the Coordination for the Improvement of Higher Education Personnel - Brasil (CAPES) - Finance Code 001. We also thank the physics laboratory at the Toledo campus of the Federal Technological University of Paraná (UTFPR).

References

[1] S. Li, X. Zhao, Z. Tao, B. Wei, W. Ding, and Q. Dai, "A simplified computational model for circadian stimulus based on illuminance, correlated color temperature, and color rendering index," IEEE Photonics Journal, vol. 14, no. 6, pp. 1–10, 2022.

[2] T. Katsuura et al., "Effects of color temperature of illumination on physiological functions," Journal of PHYSIOLOGICAL ANTHROPOLOGY and Applied Human Science, vol. 24, no. 4, pp. 321–325, 2005.

[3] X. Guo and K. Houser, "A review of colour rendering indices and their application to commercial light sources," Lighting Research & Technology, vol. 36, no. 3, pp. 183–197, 2004. [Online]. Available: https://doi.org/10.1191/1365782804li112oa

[4] K. Ito, H. Higashi, A. Hietanen, P. Fält, K. Hine, M. Hauta-Kasari, and S. Nakauchi, "The optimization of the light-source spectrum utilizing neural networks for detecting oral lesions," Journal of Imaging, vol. 9, no. 1, 2023. [Online]. Available: https://www.mdpi.com/2313-433X/9/1/7

[5] C.-C. Sun et al., "Linear calculation model for prediction of color rendering index performance associated with correlated color temperature of white light-emitting diodes with two phosphors," Light: Science & Applications, vol. 51, no. 5, pp. 233–238, 2012.

[6] N. SÁndor and J. Schanda, "Visual colour rendering based on colour difference evaluations," Lighting Research & Technology, vol. 38, no. 3, pp. 225–239, 2006. [Online]. Available: https://doi.org/10.1191/1365782806lrt168oa

[7] M. P. Royer, "IES TM-30-15 is approved—now what?" LEUKOS, vol. 12, no. 1-2, pp. 3–5, 2016. [Online]. Available: https://doi.org/10.1080/15502724.2015.1092752

[8] K. Bera, R. Parthiban, and N. Karmakar, "Coverage improvement of laser diode-based visible light communication systems using an engineered diffuser," IEEE Access, vol. 11, pp. 122 833–122 841, 2023.

[9] A. Scheeline, "How to design a spectrometer," Applied Spectroscopy, vol. 71, no. 10, pp. 2237–2252, 2017, pMID: 28644044. [Online]. Available: https://doi.org/10.1177/0003702817720468

[10] Z. Yang, M. Xue, and H. Guo, "Design method for engineering the initial structure of a spectrometer," Appl. Opt., vol. 63, no. 7, pp. 1783–1793, Mar 2024. [Online]. Available: https://opg.optica.org/ao/abstract.cfm?URI=ao-63-7-1783

[11] R. Horn, M. Rosenberger, G. Notni, A. Golomoz, R. Fütterer, and P.-G. Dittrich, "Investigation on chromatic aberrations and its potential for application in depth measurement," Measurement: Sensors, vol. 18, p. 100113, 2021. [Online]. Available: https://www.sciencedirect.com/science/article/pii/S2665917421000763

[12] F. Fambrini, D. G. Caetano, R. Arthur, Y. Iano, A. M. Santos, and G. F. Rissi, "An innovative lighting recognition system based on color rendering index and computational neural networking," in 2022 IEEE 31st International Symposium on Industrial Electronics (ISIE), 2022, pp. 735–740.

[13] G. H. Jacobs, "Primate photopigments and primate color vision." Proceedings of the National Academy of Sciences, vol. 93, no. 2, pp. 577–581, 1996. [Online]. Available: https://www.pnas.org/doi/abs/10.1073/pnas.93.2.577

[14] A. Stockman, D. I. A. MacLeod, and N. E. Johnson, "Spectral sensitivities of the human cones," J. Opt. Soc. Am. A, vol. 10, no. 12, pp. 2491–2521, Dec 1993. [Online]. Available: http://opg.optica.org/josaa/abstract.cfm?URI=josaa-10-12-2491

[15] A. Huete, "11 - remote sensing for environmental monitoring," in Environmental Monitoring and Characterization, J. F. Artiola, I. L. Pepper, and M. L. Brusseau, Eds. Burlington: Academic Press, 2004, pp. 183–206. [Online]. Available: https://www.sciencedirect.com/science/article/pii/B9780120644773500138

[16] T. Smith and J. Guild, "The C.I.E. colorimetric standards and their use," Transactions of the Optical Society, vol. 33, no. 3, pp. 73–134, jan 1931. [Online]. Available: https://doi.org/10.1088/1475-4878/33/3/301

[17] E. S. Pekins and H. Davson, "Human eye," Dec 2021. [Online]. Available: https://www.britannica.com/science/human-eye

[18] D. B. Judd, "A maxwell triangle yielding uniform chromaticity scales," J. Opt. Soc. Am., vol. 25, no. 1, pp. 24–35, Jan 1935. [Online]. Available: http://opg.optica.org/abstract.cfm?URI=josa-25-1-24

[19] D. L. MacAdam, "Projective transformations of I. C. I. color specifications," J. Opt. Soc. Am., vol. 27, no. 8, pp. 294–299, Aug 1937. [Online]. Available: http://opg.optica.org/abstract.cfm?URI=josa-27-8-294

[20] M. Planck, "The theory of heat radiation," 1914.

[21] I. E. Ashdown, "Chromaticity and color temperature for architectural lighting," Solid State Lighting II, pp. 51–60, 2002.

[22] J. Hernández-és, R. L. Lee, and J. Romero, "Calculating correlated color temperatures across the entire gamut of daylight and skylight chromaticities," Appl. Opt., vol. 38, no. 27, pp. 5703–5709, Sep 1999. [Online]. Available: http://opg.optica.org/ao/abstract.cfm?URI=ao-38-27-5703

[23] C. S. McCamy, "Correlated color temperature as an explicit function of chromaticity coordinates," Color Research & Application, vol. 17, no. 2, pp. 142–144, 1992. [Online]. Available: https://onlinelibrary.wiley.com/doi/abs/10.1002/col.5080170211

[24] J. Schanda, Colorimetry: Understanding the CIE System. New Jersey: Wiley Interscience, 2007.

[25] J. Setchell, "Colour description and communication," Colour Design, p. 219–253, 2012. [Online]. Available: https://www.sciencedirect.com/topics/engineering/metamerism

[26] M. R. Luo, CIE Chromatic Adaptation; Comparison of von Kries, CIELAB, CMCCAT97 and CAT02. Berlin, Heidelberg: Springer Berlin Heidelberg, 2014, pp. 1–8. [Online]. Available: https://doi.org/10.1007/978-3-642-27851-8_321-1

[27] CIE, "CIE 013.3-1995: Method of measuring and specifying colour rendering properties of light sources," Commission Internationale de 'Eclairage, 1995.

[28] Toshiba, Linear image sensor CCD (charge coupled device), Tokyo, 01 2019, rev. 1.2.

[29] D. Halliday, R. Resnick, and J. Walker, Fundamentals of Physics, Volume 2. Wiley, 2021.

[30] P. Dupuis, Z. O. Silalahi, I. Svensson, J. Brundin, N. I. Sinisuka, and G. Zissis, "Performance changes of energy saving lamps under lumen maintenance and switching stress test," in 2016 IEEE Industry Applications Society Annual Meeting, 2016, pp. 1–8.

[31] S. Shaikh, N. Soomro, F. Razaque Mughal, S. Soomro, N. Shaikh, and G. Abid, "Analysis of illumination lamp's performance by retrofit at university building, first international conference, iCETiC 2018," London, pp. 137–152, 07 2018.